In vivo imaging of mice auricle vessels using adaptive optical confocal fluorescence microscope

Yi He (何 益)[1,2,†,*], Zhibin Wang (王志斌)[1,2,4,†], Yuanyuan Wang (王媛媛)[3,4], Ling Wei (魏 凌)[1,2], Xiqi Li (李喜琪)[1,2], Jinsheng Yang (杨金生)[1,2], Guohua Shi (史国华)[1,2,], and Yudong Zhang (张雨东)[1,2]**

[1]*The Key Laboratory on Adaptive Optics, Chinese Academy of Sciences, Chengdu 610209, China*
[2]*The Laboratory on Adaptive Optics, Institute of Optics and Electronics, Chinese Academy of Sciences, Chengdu 610209, China*
[3]*School of Optometry and Ophthalmology and Eye Hospital, Wenzhou Medical College, Wenzhou 325035, China*
[4]*University of Chinese Academy of Sciences, Beijing 100039, China*
**Corresponding author: heyi_job@126.com; **corresponding author: ioe_eye@126.com*
Received August 15, 2015; accepted September 29, 2015; posted online October 21, 2015

Facilitated with stochastic parallel gradient descent (SPGD) algorithm for wavefront sensorless correcting aberrations, an adaptive optics (AO) confocal fluorescence microscopy is developed and used to record fluorescent signals *in vivo*. Vessels of mice auricle at 80, 100 and 120 μm depth are obtained, and image contrast and fluorescence intensity are significantly improved with AO correction. The typical 10%–90% rise-time of the metric value measured is 5.0 s for a measured close-loop bandwidth of 0.2 Hz. Therefore, the AO confocal microscopy implemented with SPGD algorithm for robust AO corrections will be a powerful tool for study of vascular dynamics in future.

OCIS codes: 110.0110, 170.0170, 170.1790, 170.0180.
doi: 10.3788/COL201513.111702.

In vivo visualizing subcutaneous vessels has an important role in biological research and medicine diagnosis, and the auricle vessel is a significant imaging window[1]. However, it is still challenging for confocal microscopy, widely used in biological research, to obtain high-depth penetration and diffraction-limited resolution images, mostly due to aberrations varying at different depths[2].

The aberrations could be compensated by the adaptive optics (AO) technique, which is a kind of active wavefront control technology and has been widely used in astronomy and vision science[3]. The typical AO system employs a wavefront sensor, such as Hartmann sensor, to measure aberrations in the imaging system and correct aberrations in a feedback loop using a wavefront corrector, such as deformable mirror (DM)[4]. When imaging vessels in deep tissue using a traditional AO system, it is relatively invalid in that the wavefront sensor would receive a multitude of wavefronts emitting from different parts of tissue to destroy the aberration correction[5,6]. An artificial guide star resulting from fluorescent beads or fluorescent protein to measure aberrations has been conducted researches in single-photon or multi-photon scanning microscopy[7,8], and has been demonstrated for *in vivo* imaging of drosophila embryos by Tao[9]. However, it is not always feasible to find appropriate fluorescent protein in different samples at different depths.

An attraction of wavefront sensorless AO with particular optimization algorithm was firstly proposed by Booth[10]. Wavefront sensorless AO systems measure an image quality metric with a group of setting trial aberrations, then operate by sequentially modulating the AO corrector and maximizing a feedback signal according to optimization algorithms[11]. Wavefront optimization algorithms have been studied in microscopy including modal method, random search algorithm, aperture segment method, genetic algorithm, hill-climbing algorithm and so on[12,13]. The main disadvantage of these optimization algorithms is a slow correction speed[14], limiting their applications in biological tissue *in vivo* imaging.

In this Letter, we propose stochastic parallel gradient descent (SPGD) algorithm for the aberration correction in an AO confocal microscopy. The SPGD algorithm was first proposed by Vorontsov[15] and has been widely used in laser beam shaping and astronomy[16]. Research has verified that SPGD was the fastest and most efficient search method for AO wavefront sensorless sytems[17]. Zernike polynomials, which are the most commonly used modes in microscopy and have certain well-known advantages compared to other modal representations[18], were chosen to be control basis of SPGD algorithm, and the aberration in pupil could be expanded as:

$$\Phi(u,v) = \sum a_i Z_i(u,v), \tag{1}$$

where $Z_i(u,v)$ is the ith Zernike polynomial with coefficient a_i. The first 22 Zernike polynomials except the first 4 polynomials are used for aberration correction in this Letter. Piston, tip, tilt, and defocus components are removed from the basis modes because they do not affect image quality but only cause offset of focus position in three directions.

Image sharpness was chosen as a metric of image quality[15]. It could be described as:

$$M = \sqrt{\frac{1}{mn}\sum_{\text{pixels}}(I(x,y) - \langle I\rangle)^2}, \tag{2}$$

where $\langle I\rangle$ is an averaged gray-level of an image with $m * n$ pixels and $I(x, y)$ is the gray of one pixel.

The SPGD algorithm could be expressed as:

$$a_i^{n+1} = a_i^n + k\delta_i^n(M^{n+} - M^{n-}), \tag{3}$$

where δ_i^n is a randomized perturbation applied for the ith control channel for the AO corrector, which is a Bernoulli distribution vector, namely the same amplitude in a randomly signed direction; M^{n+} is the metric when randomized perturbations $(\delta_1^n, \delta_2^n ... \delta_i^n, \delta_{i+1}^n ...)$ is applied for all control channels; M^{n-} is the metric when the control channels are perturbed in the opposite direction. k is the descent rate, which is namely gain coefficient, positive for finding a maximum of the image metric M. Therefore, the SPGD algorithm is an iterative scheme which makes use of Zernike coefficient a_i in Eq. (3) to very quickly find the minimizer of the aberration in pupil $\Phi(u, v)$ in Eq. (2).

Figure 1 shows the schematic diagram of the AO confocal fluorescence microscopy and a detailed description of the system configuration can be found in Ref. [19]. In brief, a laser diode (LD) with a central wavelength of 638 nm is collimated and passes through various optical components which are arranged off-plane, and then enters the objective lens (Olympus UA, water immersion, 20×, NA = 0.5, 3.5 mm working distance, Japan) which focuses it to a small spot on the specimen. Unlike the lens-based AO confocal microscope[19], spherical mirrors are used in pairs in this AO confocal fluorescence microscope, creating an afocal telescope to preserve conjugate planes, and to prevent back reflection (which is harmful in a double-pass system) and chromatic aberrations. A DM with 61-element placed at the pupil plane is used to compensate for aberrations. The two scanning mirrors (HS: 16 kHz resonant scanner, VS: 30 Hz galvometor scanner) provide two dimensions raster scanning of the focused spot of the specimen in the X and Y directions (the objective lens axis being the Z direction). Light emitted from the specimen fluorescence passes through the same optical path as the incoming beam then is collected and focused on a pinhole (30 μm size) which is conjugate to the focused spot. A photomultiplier tube (PMT, H7422-20, Hamamatsu, Japan) is placed after the pinhole to record the intensity of the scattered light for each position of the spot. By synchronizing the signal from PMT and two scanning mirrors, the images can be consecutively recorded with a frame rate of 30 Hz.

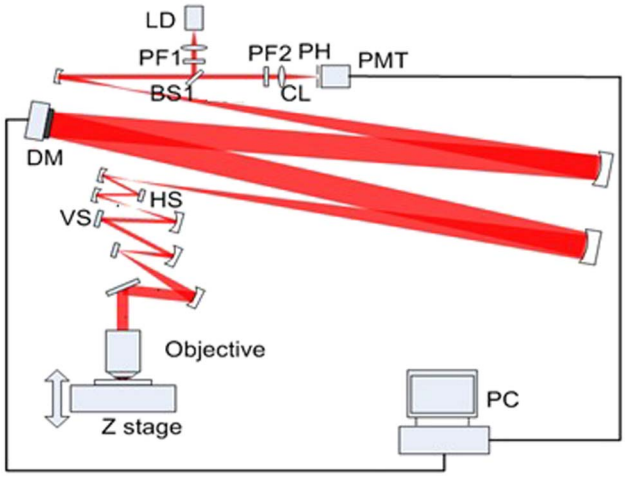

Fig. 1. Scheme of AO confocal fluorescence microscopy system. BS: beam splitter. PF: bandpass filter. HS: horizontal scanner. VS: vertical scanner. PH: pinhole. CL: collecting lens.

Before *in vivo* imaging of vessels, BALB/c-nu mice were deeply anesthetized with pentobarbital (Sagital, 80 mg/kg i.p.), and the fluorescent lipophilic tracers DiD (Molecular Probes) were injected into the tail vein[20]. The auricle vessel was then imaged using the custom-built AO confocal fluorescence microscopy while the mice was under anesthesia on a warmed microscope stage. High-resolution images were obtained at depths of hundreds of microns and axial intervals of 20 μm using the water immersion objective lens.

Fluorescence images of vessels without and with AO correction are shown in Fig. 2, which correspond to the depth at 80, 100, and 120 μm below the surface of the auricle, respectively. The images after AO correction are much brighter than the ones before correction, and one observes that there is a great enhancement of fluorescence signals in all depths of vessels. Here structure details of vessels are more abundant, since the AO correction could

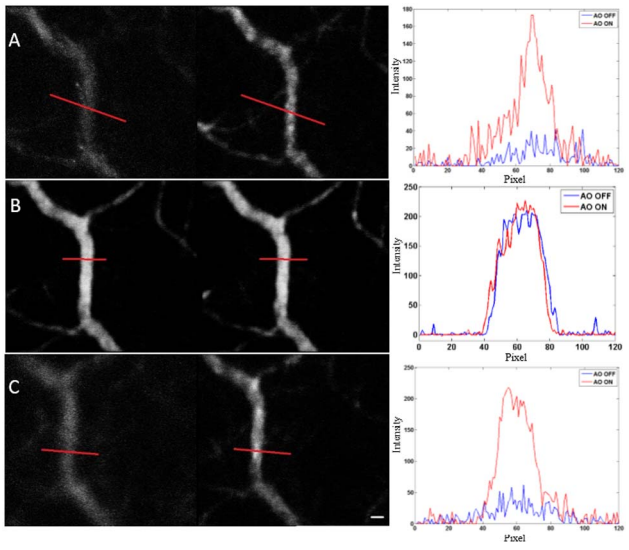

Fig. 2. Fluorescence images without and with AO correction at different depth, and fluorescence signal profiles corresponding to each depth: (A) 80, (B) 100, and (C) 120 μm. The image size is $314 * 314$ microns with a scale bar of 10 μm.

improve the transverse resolution of the microscope and enhance image contrast.

To manifest the enhancement of resolution and contrast with AO correction, the fluorescence signal profiles of the red dashed line of Figs. 2(A)–2(C) are plotted on the right side. The peak intensity increases by 4.6×, and 4.2× for the depth of 80 and 120 μm in Figs. 2(A) and 2(C), respectively. At the depth of 100 μm in Fig. 2(B), the intensity enhancement is hard to distinguish. One possible reason for the variability of the improvement is that the aberration is not spatially invariant over the field, and the best focused depth is on the 100 μm below the surface of the auricle. However, finer details of vessels in the right part of Fig. 2(B) is shown more clearly after AO correction, and the image is a little brighter then.

The metric values of images during AO correction process are plotted in Fig. 3. Note that we focus on the vessel with a central depth of 100 μm of the mice auricle, and it is a common observation that imaging resolution and contrast degrade with the increase of defocus depth. With a best focus depth of 100 μm in Fig. 2(B), the metric value of images increase to a certain stability after less than 100 iteration times, and a measured close-loop bandwidth of 0.5 Hz is achieved. For depths of 80 and 120 μm, the metric value increase 25% and 60% after almost 250 iteration times, respectively. Therefore, a typical close-loop bandwidth of 0.2 Hz is obtained with a 10%–90% rise-time of the metric value in Fig. 3. This bandwidth, although not high, is sufficient to compensate for the majority of refractive index mismatching aberrations and tissue aberrations.

In conclusion, we develop an AO confocal fluorescence microscope which can perform vessel imaging in real-time. Benefit from the AO correction with SPGD algorithm, the custom-built AO confocal fluorescence microscope is ideally suited for *in vivo* and long-term vessel imaging, since the sensorless AO confocal microscope has a simpler system architecture and can correct aberrations resulting from biological tissues in different depths non-invasively, which is very important in the field of microscope. With a robust convergence of AO correction using SPGD algorithm, improved resolution and contrast are achieved for *in vivo* fluorescence imaging of mice vessels at a depth of 80, 100, 120 μm below the surface of the auricle, and capillary morphology is more clearly, and finer vessel structures can be observed clearly.

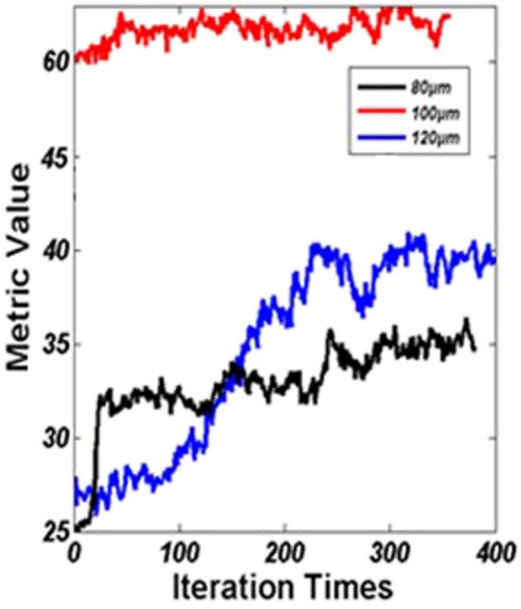

Fig. 3. Metric value of images during AO correction process in Fig. 2.

To conclude, the application of SPGD algorithm in an AO confocal fluorescence microscopy is proposed. We demonstrate the validity and accuracy of SPGD algorithm for fluorescence imaging of mice auricle vessels *in vivo*. Using image sharpness as the optimization metric in Zernike polynomial modes, a typical 10%–90% rise-time of the metric value measured is 5.0 s (150 close-loop frame times) for a measured close-loop bandwidth of 0.2 Hz. Actually, a best focused depth of 100 μm achieves a close-loop bandwidth of nearly 0.5 Hz (60 close-loop frame times). Therefore, AO with SPGD correction can greatly expand the application of confocal microscope, and will play an important role for study of many physiological imaging techniques *in vivo*.

This work was supported by the Outstanding Young Scientists of the Chinese Academy of Sciences, the National Instrumentation Program (No. 2012YQ120080), the Zhejiang Province Technology Program (No. 2013C33170), the National Science Foundation of China (No. 61108082), the Sichuan Youth Science & Technology Foundation (No. 2013JQ0028), and the West Light Foundation of the Chinese Academy of Sciences. The authors would like to thank Hao Li and Jing Lu for many helpful discussions regarding this project.

[†]These authors contributed to the work equally and should be considered co-first authors.

References

1. P. Török, S. Hewlett, and P. Varga, J. Microsc. **188**, 158 (1997).
2. M. Schwertner, M. Booth, and T. Wilson, Opt. Express **12**, 6540 (2004).
3. J. Wenhan, Acta Opt. Sin. **8**, 441 (1988).
4. J. Wenhan and L. Huagui, Proc. SPIE **1237**, 64 (1990).
5. M. Booth, M. Neil, and T. Wilson, J. Microsc. **192**, 90 (1998).
6. L. Sherman, J. Y. Ye, O. Albert, and T. B. Norris, J. Microsc. **206**, 65 (2002).
7. A. J. Wright, D. Burns, B. A. Patterson, S. P. Poland, G. J. Valentine, and J. M. Girkin, Micros. Res. Tech. **67**, 36 (2005).
8. N. Ji, T. R. Satoa, and E. Betziga, Proc. Natl. Acad. Sci. U.S.A. **109**, 22 (2011).
9. X. Tao, B. Fernandez, O. Azucena, M. Fu, D. Garcia, Y. Zuo, D. C. Chen, and J. Kubby, Opt. Lett. **36**, 1062 (2011).
10. D. Débarre, E. J. Botcherby, T. Watanabe, S. Srinivas, M. J. Booth, and T. Wilson, Opt. Lett. **34**, 2495 (2009).
11. A. Facomprez, E. Beaurepaire, and D. Debarre, Opt. Express **20**, 2598 (2012).

12. B. Ding and J. Yu, Chin. Opt. Lett. **13**, 041101 (2015).
13. Y. Yu and Y. Zhang, Chin. Opt. Lett. **12**, 121202 (2014).
14. Y. Huang, H. Yang, X. Shen, Y. Wang, L. Zheng, H. Li, and S. Xie, Chin. Opt. Lett. **10**, s11701 (2012).
15. M. A. Vorontsov and V. P. Sivokon, JOSA A **15**, 2745 (1998).
16. X. Lei, B. Xu, P. Yang, L. Dong, W. Liu, and H. Yan, Chin. Opt. Lett. **10**, 021401 (2012).
17. G. W. Carhart, J. C. Ricklin, V. P. Sivokon, and M. A. Vorontsov, in *Optical Science, Engineering and Instrumentation'97* (1997), 221.
18. Z. Wang, G. Shi, and Y. Zhang, Chin. Opt. Lett. **12**, s11103 (2014).
19. Z. Wang, D. Wei, L. Wei, Y. He, G. Shi, X. Wei, and Y. Zhang, J. Biomed. Opt. **19**, 086009 (2014).
20. C. L. Celso, J. W. Wu, and C. P. Lin, J. Biophoton. **2**, 619 (2009).